

# Improving the precision of weak-value-amplification with two cascaded Michelson interferometers based on Vernier-effect

Jing-Hui Huang<sup>1,\*</sup>, Fei-Fan He<sup>1,†</sup>, Xue-Ying Duan<sup>2,3,4,‡</sup>, Guang-Jun Wang<sup>2,3,4,§</sup> and Xiang-Yun Hu<sup>1,¶</sup>

<sup>1</sup> School of Institute of Geophysics and Geomatics,

China University of Geosciences, Lumo Road 388, 430074 Wuhan, China.

<sup>2</sup> School of Automation, China University of Geosciences, Lumo Road 388, 430074 Wuhan, China.

<sup>3</sup> Hubei Key Laboratory of Advanced Control and Intelligent Automation for Complex Systems, China and

<sup>4</sup> Engineering Research Center of Intelligent Technology for Geo-Exploration, Ministry of Education, China

A modified-weak-value-amplification(MWVA) technique of measuring the mirror's velocity based on the Vernier-effect has been proposed. We have demonstrated with sensitivity-enhanced and the higher signal-to-noise ratio(SNR) by using two cascaded Michelson interferometers. These two interferometers are composed of similar optical structures. One interferometer with a fixed mirror acts as a fixed part of the Vernier-scale, while the other with a moving mirror acts as a sliding part of the Vernier-scale for velocity sensing. The envelope of the cascaded interferometers shifts much more than a single one with a certain enhancement factor, which is related to the free space range difference between these two interferometers. In addition, we calculate the SNR based on the Fisher information with both the MWVA technique and the traditional-weak-value-amplification(TMVA) technique. The results show that the SNR with our MWVA technique is larger than the the SNR with the TWVA technique within the range of our time measurement window. Our numerical analysis proved that our MWVA technique is more efficient than the TWVA technique. And by using the principles of the Vernier-effect, it is applicative and convenient to ulteriorly improving the sensitivity and SNR in measuring other quantities with the MWVA technique.

## I. INTRODUCTION

A weak measurement is a new tool for characterizing post-selected quantum systems in the recent development of quantum mechanics[1, 2]. Historically speaking, the idea of this measurement was originally proposed by Aharonov, Albert and Vaidman[3] as an extension to the standard("projective") von-Neumann model of measurement. In weak measurement, information is gained by weakly probing the system, while approximately preserving its initial state. The average shift of the final pointer state can go far beyond the eigenvalue spectrum of the system observable in sharp contrast to the standard quantum measurement. This average shift is called the weak value, which is usually complex[4, 5]. These features have allowed a wide range of applicability in understanding many counter-intuitive quantum results. For example, weak value can offer new insights into quantum paradox, such as Hardy's paradox[6, 7], the three-box paradox[8], apparent superluminal travel[9], direct measuring the real and imaginary components of the wavefunction [10].

In addition to the fundamental physics interest in weak values, one of the major goals in weak measurement is to enhance the sensitivity of estimating weak signals[11–15]. For example, Dixon et al. amplified very small transverse deflections of an optical beam, then measured the angular

deflection of a mirror down to  $400 \pm 200$  frad and the linear travel of a piezo actuator down to  $14 \pm 7$  fm [16]. Boyd et al. demonstrated the first realization of weak-value amplification in the azimuthal degree of freedom and had achieved effective amplification factors as large as 100[12]. Viza et al. achieved a velocity measurement of 400 fm/s by measuring one Doppler shifted due to a moving mirror in a Michelson interferometer[17]. Pati et al. even proposed an alternative method to measure the temperature of a bath using the weak measurement scheme with a finite-dimensional meter[18]. Therefore, these applications have been termed as the weak-value-amplification(WVA) technique in literature[19].

It is worth noting that weak-value-amplification cannot be arbitrarily large in the cost of decreasing output laser intensity[20]. The analysis of Koike et al.[21] showed that the measured displacement and the amplification factor are not proportional to the weak value and rather vanish in the limit of infinitesimal output intensity. The work of Pang et al.[22] investigated the limiting case of continuous-variable systems to demonstrate the influence of system dimension on the amplification limit. Therefore, it is still the focus in weak measurement to enhance the sensitivity of detecting small signals. The experiment of Starling et al.[23] and the proposal of Feizpour et al. [24] showed that post-selection can significantly raise the signal-to-noise ratio (SNR) of weak measurement. Huang et al[25] proposed an approach called dual weak-value amplification (DWVA), with sensitivity several orders of magnitude higher than the standard approach without losing signal intensity. Krafczyk et al[26]. experimentally demonstrated recycled weak-value measurements. By using photon counting detectors, they demonstrated a signal improvement by a factor of  $4.4 \pm 0.2$  and a signal-

\* Email:jinghuihuang@cug.edu.cn

† Email:hfeifan2017@cug.edu.cn

‡ Email:CUGxyDuan@163.com

§ Email:gjwang@cug.edu.cn

¶ Email:xyhu@cug.edu.cn

to-noise ratio improvement of  $2.1 \pm 0.06$ , compared to a single-pass weak-value experiment.

Recently, Vernier-effect has been an effective tool to enhance the sensitivity of photonic devices[27–30]. The Vernier-effect is an efficient method to enhance the accuracy of measurement instruments, which consists of two/three scales with different periods. In Ref.[27] a sensor is introduced that consists of two cascaded ring resonators, and it is shown theoretically that it can obtain very high sensitivities thanks to the Vernier principle. In [29] a high sensitivity of 1892dB/RIU of the optical sensor was achieved for the intensity interrogation based on the cascaded reflective Mach–Zehnder interferometer(MZI)s and the micro-ring resonators. Further, in Ref.[30] a three cascaded micro-ring resonators based refractive index optical sensor with a high sensitivity of 5866 nm/RIU was demonstrated, the measurement range of which is significantly improved 24.7 times compared with the traditional two cascaded micro-ring resonators.

In this letter, we put forward a modified-weak-value-amplification(MWVA) with two cascaded Michelson interferometers to improve the sensitivity of traditional-weak-value-amplification(TMVA) based on the Vernier-effect. More specifically, in the framework of quantum weak measurements, we observe the temporal shift induced by a small spectral shift with two cascaded Michelson interferometers. The spectral shift in our scheme is a Doppler frequency shift produced by a mirror in one of the interferometers, while the other interferometer has the same optical structure with no movement of the mirror. By numerical simulation, We obtain the temporal shift dependence of the velocity, the sensitivity, and the signal-to-noise ratio (SNR) calculated from the Fisher information[31]. Besides, our MWVA technique is comparable to the TWVA technique, but allows us to reach the higher sensitivity and SNR under the same conditions of measuring time.

The paper is organized as follows. In Sec II.A, we briefly review the TWVA technique for measurement velocity in a single Michelson interferometer. Then, in Sec II.B, we first derive the MWVA technique for the velocity with two cascaded Michelson interferometers based on Vernier-effect. In Sec III, by ensuring the same time measurement window and determine the respective meter in the two techniques, we obtained analytic results of the sensitivity and the SNR from the Fisher information. Sec IV is devoted to the summary and the discussions.

## II. THE TWVA TECHNIQUE AND THE MWVA TECHNIQUE

In this article, we propose and numerically demonstrate a weak measurement scheme, in which the amplification of the phase shifts in a Michelson interferometer can be effectively enhanced by introducing another cascaded interferometer based on the Vernier-effect. In order to compare our new technique to the traditional

ones, we briefly review the traditional WVA technique to measuring velocity with a Michelson interferometer by following the Ref.[17] in the following subsection.

### A. The WVA technique for velocity measurements

In this section, we briefly review an interferometer scheme in Ref.[17] combined WVA technique to measure longitudinal velocities with the temporal meter. The temporal shift is proportional to the weak value and can be amplified in the measurement of  $v$ , which is accompanied by a decrease in the measured intensity due to the nature of the weak measurement. The temporal shift is induced by the spectral shift, which is a Doppler frequency shift produced by a moving mirror in a Michelson interferometer. The weak measurement is characterized by state preparation, a weak perturbation, and post-selection. The detail of the WVA technique for velocity measurements is shown in Fig. 1.

The TWVA technique of weak measurement can be characterized into three parts: state preparation, weak interaction, and post-selection. The initial state  $|\Phi_i\rangle$  of the system and  $|\Psi_i\rangle$  of the meter are prepared with the polarizer and AO Modulator. The initial polarization state of the system can be described by the polarization qubit:

$$|\Phi_i\rangle = \sin(\alpha)|H\rangle + \cos(\alpha)|V\rangle \quad (1)$$

where  $\alpha = \pi/4$  is the angle between the horizontal line and the transmission axis of line polarizer(pre-selection); The horizontal polarization state  $|H\rangle$  correspond to the arm with the mirror which the light goes through, while the vertical polarization state  $|V\rangle$  correspond to the arm with piezo-driven mirror in the Michelson interferometer. The preparation of the meter consists of the generation of the temporal mode

$$I_{single}^i = |\langle p|\Psi_i\rangle|^2(t) = \frac{1}{\sqrt{2\pi\tau^2}} e^{-(t+t_0)^2/2\tau^2} \quad (2)$$

where  $\tau$  is the length of the Gaussian pulse and  $t_0$  is the center of the pulse. The advantage of that temporal meter and the non-Fourier limited Gaussian-shaped pulse has been studied in Ref.[17]. The pulse is injected into a Michelson interferometer, where the horizontally polarized component of the pulse goes through the arm with a slowly moving mirror at speed  $v$ , and the vertically one goes through the arm with a piezo-Driven mirror. The weak interaction in Fig. 1 can be expressed as

$$U = e^{-ig\hat{A}\otimes\hat{p}} = e^{-i\omega_d\hat{A}t/2} \quad (3)$$

where  $\omega_d = 2\pi f_d = 2\pi\frac{2v}{\lambda}$ . Note that the spectral shift  $f_d = 2v/\lambda$  is proportional to velocity  $v$ . The observable  $\hat{A}$  satisfies:  $\hat{A} = \frac{1}{2}(|H\rangle\langle H| - |V\rangle\langle V|)$ .

Finally, the post-selection of the weak measurement is controlled by inducing a phase offset  $2\phi$  by the piezo-

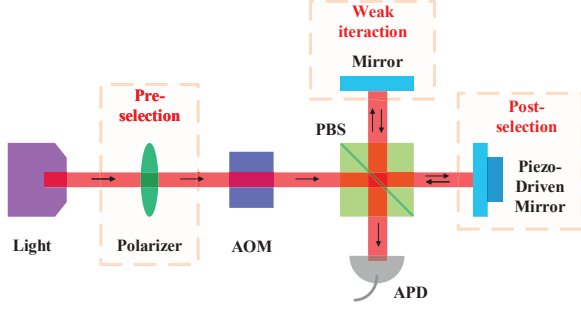


FIG. 1. Schematic of the WVA technique for velocity measurements in the single Michelson. AOM is the Acousto-Optic Modulator, which can modulate the light into a temporal Gaussian shaped pulse. PBS is the polarizer beam splitter. The arrival time of single photons is measured with an avalanche photodiode(APD).

Driven mirror. Thus, the final post-selection of the system is given by:

$$|\Phi_f\rangle = \frac{1}{\sqrt{2}}(|H\rangle - e^{i2\phi}|V\rangle) \quad (4)$$

and the weak value can be calculated by:

$$A_w = \frac{\langle\Phi_f|\hat{A}|\Phi_i\rangle}{\langle\Phi_f|\Phi_i\rangle} = -i\cot\phi \approx \frac{-i}{\phi}, \quad (5)$$

By following the original work in Ref.[3], the meter state of the temporal mode after the post-selection becomes:

$$\begin{aligned} \langle p|\Psi_f\rangle &= \langle\Phi_f|U|\Phi_i\rangle\langle p|\Psi_i\rangle \\ &= \langle\Phi_f|e^{-ig\hat{A}\otimes\hat{p}}|\Phi_i\rangle\langle p|\Psi_i\rangle \\ &= \langle\Phi_f|\Phi_i\rangle[1 - igA_w\hat{p}] \langle p|\Psi_i\rangle + O(g^2) \\ &\approx \langle\Phi_f|\Phi_i\rangle e^{-igA_w\hat{p}} \langle p|\Psi_i\rangle \end{aligned} \quad (6)$$

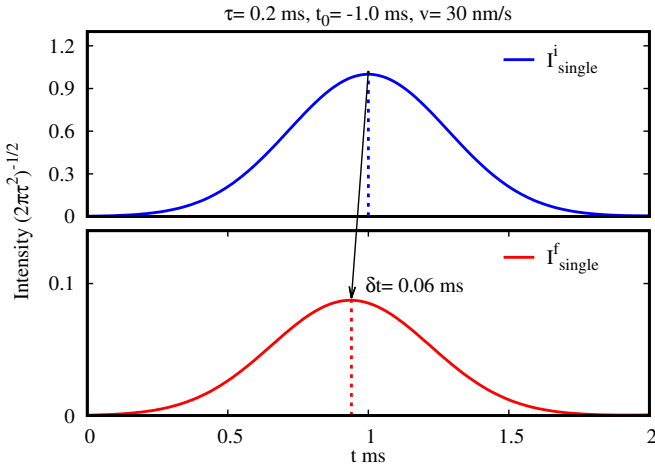


FIG. 2. The time shift of meter in the scheme of the WVA technique for measuring velocity  $v = 30$  nm/s with the length of the Gaussian pulse  $\tau = 0.2$  ms and the phase offset  $\phi = 0.3$  rad of the post-selection. The vertical dot line represents the corresponding the center of the Gaussian function.

and therefore, the absolute value squared of the meter state (6) is given by:

$$\begin{aligned} I_{single}^f &= |\langle p|\Psi_f\rangle|^2 \\ &= (\sin\phi)^2 e^{-\frac{2\pi vt}{\lambda\phi}} |\langle p|\Psi_i\rangle|^2 \\ &= \frac{(\sin\phi)^2}{\sqrt{2\pi\tau^2}} e^{-\frac{2\pi vt}{\lambda\phi}} e^{-(t+t_0)^2/2\tau^2} \\ &\approx \frac{(\sin\phi)^2}{\sqrt{2\pi\tau^2}} e^{-(t+t_0+\frac{4\pi\tau^2 v}{\lambda\phi})^2/2\tau^2} \end{aligned} \quad (7)$$

The final step approximation of Eq.(7) condition is  $4\pi v\tau^2 \ll \lambda\phi$ . In the scheme of the traditional WVA technique for measuring velocity, the time shift  $\delta t = \frac{4\pi\tau^2 v}{\lambda\phi}$  in Eq.(7) is amplified in the measurement of  $v$ . Note that the work in Ref.[17] and our derivation show that the spectral shift  $f_d = 2v/\lambda$  can translate into the time shift  $\delta t = \frac{2\pi\tau^2 f_d}{\phi} = \frac{4\pi\tau^2 v}{\lambda\phi}$ .

In addition, we show the time shift of meter in the scheme of the TWVA technique for measuring velocity  $v = 30$  nm/s with the length  $\tau = 0.2$  ms and central wavelength  $\lambda = 800$  nm of the Gaussian pulse in Fig. 2. Note that the work in Ref.[32] studied an interferometric scheme based on a purely imaginary weak value, combined with a frequency-domain analysis, which may have the potential to outperform standard interferometry by several orders of magnitude. However, the amplification of the TWVA technique can not be arbitrarily large due to the limit of the resolution of the detector. Therefore, the MWVA technique based on Vernier-effect with two cascaded Michelson interferometers for measuring velocity is proposed in the next subsection.

## B. The MWVA technique based on Vernier-effect

In this section, we propose a sensitivity-enhanced scheme of the MWVA technique with two cascaded Michelson interferometers based on the Vernier-effect. In addition, through numerical simulation experiments, we verify the effectiveness and feasibility of the MWVA technique.

The schematic diagram of the MWVA technique for measuring velocity is shown in Fig. 3. It includes two Michelson interferometers based on the TWVA technique, and each Michelson interferometer is the same as the Michelson interferometer with the TWVA technique in Fig. 1. The upper interferometer with moving mirror 1 serves as the sliding part of the Vernier-scalar, as the velocity changes will cause a shift of the final meter. The lower interferometer with static mirror 2 serves as the fixed part of the Vernier-scalar. The Vernier-scale is an efficient method to enhance the accuracy of measurement instruments, which consists of two scales with different periods[33].

In our work, the upper interferometer and the lower interferometer are prepared with different free spectrum

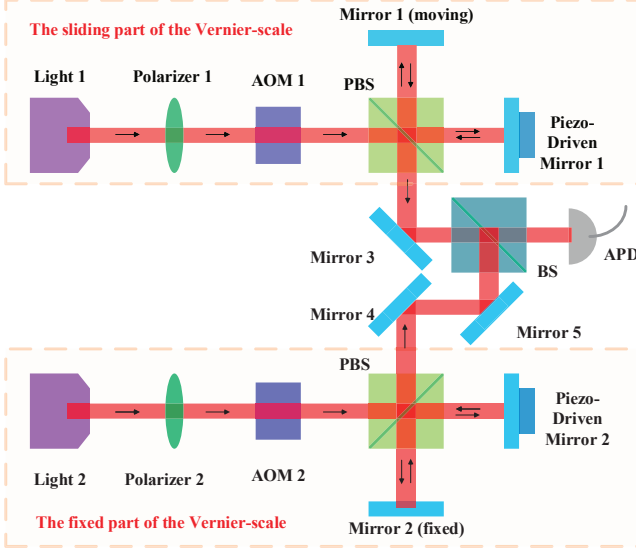


FIG. 3. The scheme of the MWVA technique with two cascaded Michelson interferometers based on Vernier-effect.

range(FSR). The total transmission meter of the cascaded Michelson interferometer is the superposition of the optical power output of two interferometers, which exhibits peaks at times where two interference peaks of the respective interferometers partially overlap. The envelope period is given by

$$\frac{FSR_{sliding} \times FSR_{fixed}}{|FSR_{sliding} - FSR_{fixed}|} \quad (8)$$

When the velocity change, the transmission of the single(upper) interferometer will shift. Then the shift of cascaded Michelson interferometers envelope is magnified by a certain factor  $Enh$ . The shift of the transmission peak is proportional to the enhanced factor

$$Enh = \frac{FSR_{fixed}}{|FSR_{sliding} - FSR_{fixed}|} \quad (9)$$

In order to produce the Vernier-effect, the parameters of the main optical components in our scheme in Fig. 3 shall meet the following requirements:

(i) **Light**: high-power light source is suitable for our scheme. Note that the pulses for light 1 and light 2 don't have to be coherent, because the laser detected at APD is the superposition of the optical power output of two interferometers.

(ii) **Piezo -Driven Mirror**: the post-selection of the TWVA technique is controlled by inducing a phase offset  $2\phi$  with the Piezo-Driven Mirror. In other words, the intensity of the outgoing light is proportional to the phase offset  $2\phi$ , which is shown in Eq.(7). To obtain the overlap with easily discernible peaks, the intensity of the outgoing light of each interferometer, namely the phase offset  $2\phi$  should keep the same value.

(iii) **AOM**: AOM is the most critical device in our scheme. According to the researches in Ref. [29, 30, 33],

the pulse, which serves as the sliding part or the fixed part of the Vernier-scale, ought to be produced with equally spaced Gaussian mode rather than individual pulse (2). At the same time, AOM is mainly used outside the laser cavity, using the electric signal of the driving source to modulate the laser[34]. In our work, AOM 1 modulates the laser with  $FSR_{sliding}$  as the pre-selection meter  $|\langle p|\Psi_i \rangle|_{sliding}^2(t) = I_u^i$  in upper interferometer, while AOM 2 modulates the laser with  $FSR_{fixed}$  as the pre-selection meter  $|\langle p|\Psi_i \rangle|_{fixed}^2(t) = I_d^i$  in lower interferometer. Then  $I_u^i$  and  $I_d^i$  are given by:

$$I_u^i = \sum_{m=0}^N \frac{1}{\sqrt{2\pi\tau^2}} e^{-(t+t_0-m \times FSR_{sliding})^2/2\tau^2} \quad (10)$$

$$I_d^i = \sum_{m=0}^N \frac{1}{\sqrt{2\pi\tau^2}} e^{-(t+t_0-m \times FSR_{fixed})^2/2\tau^2} \quad (11)$$

The final meter  $|\langle p|\Psi_f \rangle|_{fixed}^2(t) = I_d^f$  of the lower interferometer becomes:

$$I_d^f = \sum_{m=0}^N \frac{(\sin\phi)^2}{\sqrt{2\pi\tau^2}} e^{-(t+t_0-m \times FSR_{fixed})^2/2\tau^2} \quad (12)$$

The final meter  $|\langle p|\Psi_f \rangle|_{sliding}^2(t) = I_u^f$  of the upper interferometer with moving mirror 1 at velocity  $v$  becomes:

$$I_u^f = \sum_{m=0}^N \frac{(\sin\phi)^2}{\sqrt{2\pi\tau^2}} e^{-(t+t_0-m \times FSR_{sliding} + \frac{4\pi\tau^2 v}{\lambda\phi})^2/2\tau^2} \quad (13)$$

The intensity  $I_{sum}^f = I_u^f + I_d^f$  of the total laser detected at APD is the sum of the light power  $I_u^f$  from the upper interferometer and the light power  $I_d^f$  from the lower interferometer.

In the end, we fix a specific experimental setup, that is, the given chosen post-selection phase  $\phi = 0.3$  rad, the length  $\tau = 0.2$  ms and central wavelength  $\lambda = 800$  nm, the parameter  $t_0=0.0$  of the pulse  $I_u^i$  (10) and the pulse  $I_d^i$  (11), the free spectrum range  $FSR_{fixed}=2.0$  ms of the lower interferometer and the free spectrum range  $FSR_{sliding}=1.96$  ms of the upper interferometer in Fig. 3, so that numerical simulation of the transmission temporal shift of single Michelson interferometer is shown in Fig. 4(a), and numerical simulation of the transmission temporal shift of two cascaded Michelson interferometers is shown in Fig. 4(b). Then the sensitivity-enhanced factor  $Enh = \frac{3 \text{ ms}}{0.06 \text{ ms}} = 50$  due to the Vernier-effect, which is the same value as the value  $Enh = \frac{2.00 \text{ ms}}{2.00 \text{ ms} - 1.96 \text{ ms}} = 50$  calculated from Eq. (9). The results verify that the sensitivity for measuring velocity can be enhanced much more according to the calculated sensitivity-enhanced factor (9) by choosing two interferometers with smaller differences in FRS. However, in practice, there is a compromise between the sensitivity and measurement accuracy. Because the smaller FRS difference will increase the FRS of the envelope, which introduces the difficulty in tracking the temporal shift of the envelope peak [33].



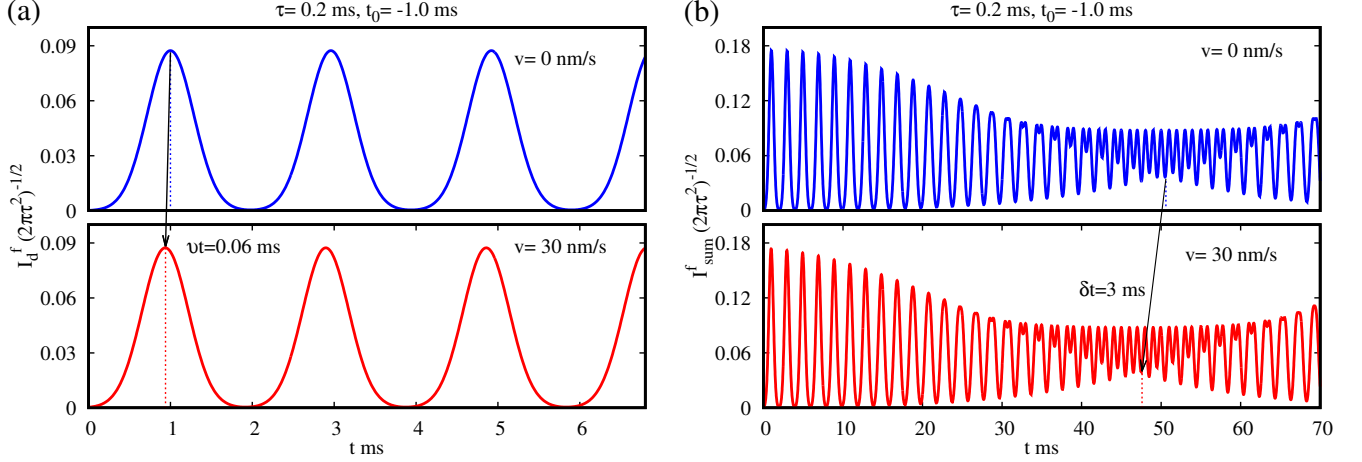


FIG. 4. Numerical simulation of the transmission temporal shift of (a) single Michelson interferometer and (b) two cascaded Michelson interferometers.

The numerical results show that the MWVA technique based on Vernier-effect is more sensitive than the TWVA technique despite how much time is used in the two techniques. In the scheme of the TWVA technique, Eq.(7) indicates that time shift  $\delta t = \frac{4\pi\tau^2 v}{\lambda\phi}$  can be effectively enhanced by increasing the measuring time. Meanwhile, the Fig. 4. show that our scheme costs more time than the scheme of the single Michelson interferometer. Therefore, our work leads to a new issue: is the MWVA technique based on Vernier-effect more sensitive than the TWVA technique at the same measurement time? And further discussion is shown in the next section.

### III. FURTHER DISCUSSIONS AND NUMERICAL RESULTS

#### A. The sensitivity-enhanced factor at the same measurement time

In this subsection, we will study the sensitivity-enhanced factor in the two schemes mentioned above at the same measurement time. Note that we can obtain the temporal shift in a certain and effective time window, and the rest time window is useless in the measurement. For example, When time is greater than 2 ms of the window in Fig. 4(a), the measurement is invalid.

In the next step, by choosing the appropriate meter in the TWVA technique and the MWVA technique, we compare the sensitivity of these techniques at the same measurement time. Note that we can obtain the temporal shift in a certain and effective time window. The simulation is shown in Fig. 5. The  $I_u^i$  and  $I_d^i$  are chosen with chosen post-selection phase  $\phi = 0.3$  rad, the length  $\tau=0.2$  ms of the individual Gaussian pulse, the parameter  $t_0=46.0$  of the pulse  $I_u^i$  (10) and the pulse  $I_d^i$  (11), the free spectrum range  $FSR_{fixed}=2.0$  ms of the lower interferometer and the free spectrum range  $FSR_{sliding}=1.96$

ms of the upper interferometer in Fig. 3. Then  $I_u^i$  and  $I_d^i$  are given by

$$I_d^i = \begin{cases} \sum_{m=0}^N \frac{1}{\sqrt{2\pi \times 0.2^2}} e^{-(t+46-2.00m)^2/(2 \times 0.2^2)} & t < 4ms \\ 0 & t > 4ms \end{cases}$$

$$I_u^i = \begin{cases} \sum_{m=0}^N \frac{1}{\sqrt{2\pi \times 0.2^2}} e^{-(t+46-1.96m)^2/(2 \times 0.2^2)} & t < 4ms \\ 0 & t > 4ms \end{cases}$$

In order to keep the same measurement time, the meter mode  $I_{single}^i$  (2) of the schematic of the TWVA technique with the single Michelson in Fig. 1 should be modulated with the length  $\tau=0.4$  ms and the length  $t_0=-2.0$  of the Gaussian pulse. The  $I_{single}^i$  is given by:

$$I_d^i = \begin{cases} \frac{1}{\sqrt{2\pi \times 0.4^2}} e^{-(t-2.0)^2/(2 \times 0.4^2)} & t < 4ms \\ 0 & t > 4ms \end{cases}$$

With the input of the  $I_{single}^i$  of the single Michelson in Fig. 1, we can obtain the final meter  $I_{single}^f$  (7) of measuring velocity  $v=30$  nm/s and  $v=10$  nm/s in Fig. 5(a) and Fig. 5(c). Under the same window of measurement time, the results of the detected intensity  $I_{sum}^f$  of the two cascaded Michelson interferometers measuring velocity  $v=30$  nm/s and  $v=10$  nm/s based on Vernier-effect are shown in Fig. 5(b) and Fig. 5(d).

The method of how to chose the window of measurement time is explained as follows. The selected goal is to obtain the envelope through movement of  $I_{sum}^f$  within the smallest possible measurement time window. In our work, we find that the intersection of straight lines determined by the interval troughs can track the shift of the envelope trough. More specifically, the shift of  $I_{sum}^f$  can be calculated by tracking the shift of the trough, which is the nearest wave to the right of the intersection. Therefore, we call the above method the intersecting-point-tracing(IPT) method. By the IPT method, we obtain the

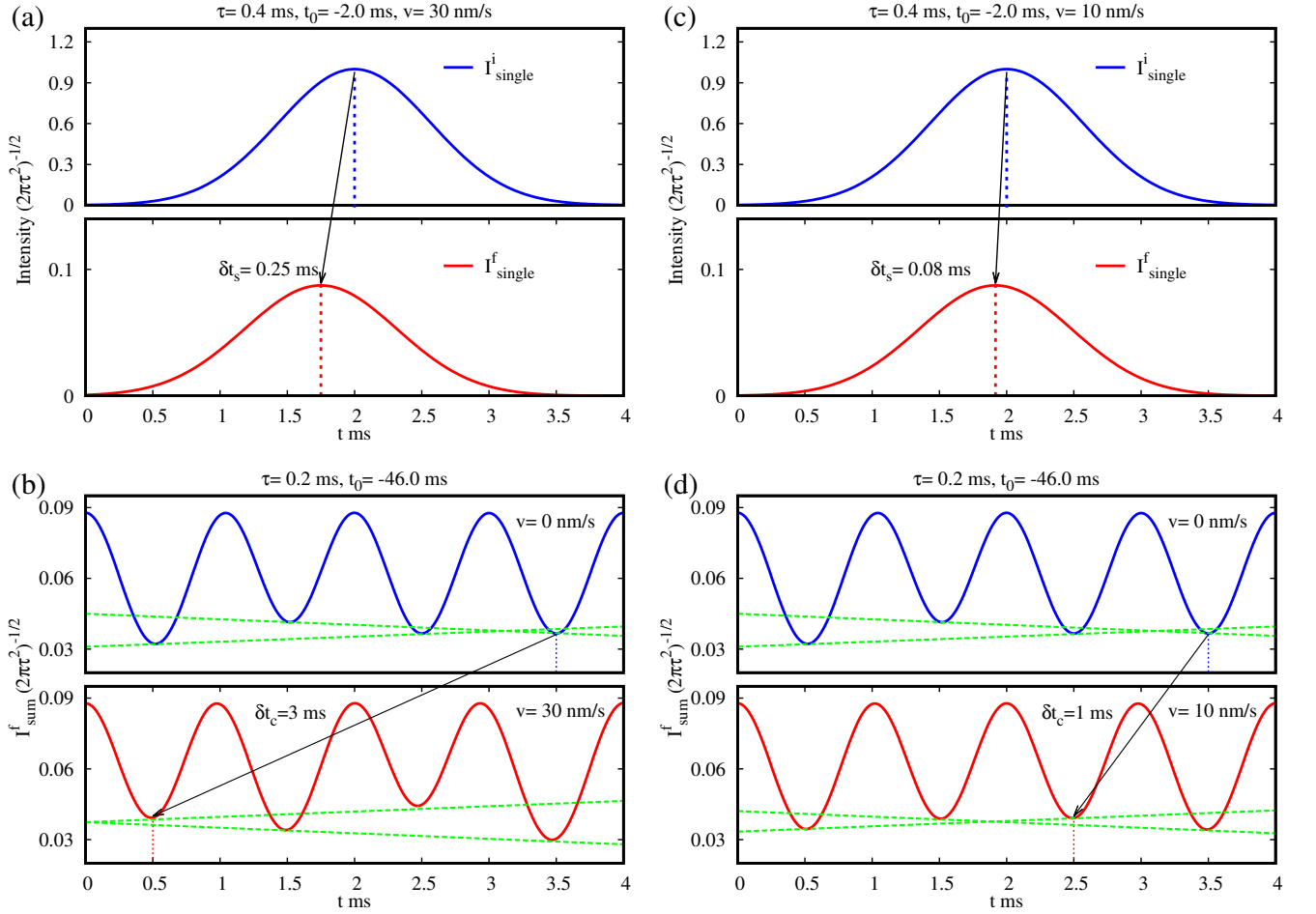


FIG. 5. Numerical simulation of the transmission temporal shift of (a) single Michelson interferometer and (b) two cascaded Michelson interferometers for measuring velocity  $v = 30$  nm/s (left plane) and velocity  $v = 10$  nm/s (right plane). The unit of the y-coordinate of each graph is  $(2\pi\tau^2)^{-1/2}$ .

shifts of the envelope  $I_{\text{sum}}^f$  at measuring velocity  $v = 30$  nm/s and  $v = 10$  nm/s based on Vernier-effect are shown in Fig. 5(b) and Fig. 5(d). And the results show that the IPT method is effective and convenient for tracking the shifts.

We can obtain the effective sensitivity-enhanced factor  $eEnh$  of measuring velocity  $v = 30$  nm/s from Fig. 5(a) and Fig. 5(c).  $eEnh$  is calculated by  $eEnh = \frac{3.00 \text{ ms}}{0.25 \text{ ms}} = 12$ . In addition, the temporal shifts of measuring velocity  $v = 10$  nm/s in Fig. 5(b) and Fig. 5(d) conclude the same result  $eEnh = \frac{1.00 \text{ ms}}{0.08 \text{ ms}} = 12$ . Though the effective sensitivity-enhanced factor  $eEnh = 12$  is smaller than the sensitivity-enhanced factor  $Enh = 50$  calculated from Eq. (9), the sensitivity of the TWVA technique for velocity measurements is still enhanced by several orders of magnitude thanks to the Vernier-effect.

In the actual measurement process, for the temporal shift to be measurable, we require that  $\delta t > \Delta t$ , where  $\Delta t$  is the resolution of the detector. Assuming that the shift  $\delta t = 0.08$  ms in Fig. 5(c) has reached the resolution  $\Delta t$  and the  $\delta t$  can not be measured. However the shift

$\delta t = 1.0 \text{ ms} > \Delta t$  in Fig. 5(d) can be effectively measured due to the sensitivity-enhanced of Vernier-effect. Therefore, the MWVA technique based on Vernier-effect can break the resolution limit of the detector of the TWVA technique for velocity measurements.

## B. The analysis of the signal-to noise ratio based on the Fisher information

In this subsection, by calculation the cramer-Rao bound (CRB) [35, 36], we consider the fundamental limitation of velocity measurements with both the traditional WVA technique and the modified WVA technique based on the Vernier-effect. The CRB is the fundamental limit in the minimum uncertainty for parameter estimation. And the CRB is equal to the inverse of the Fisher information. In information theory, for a parameter  $\Omega$  dependent probability distribution of a random variable  $x$ ,

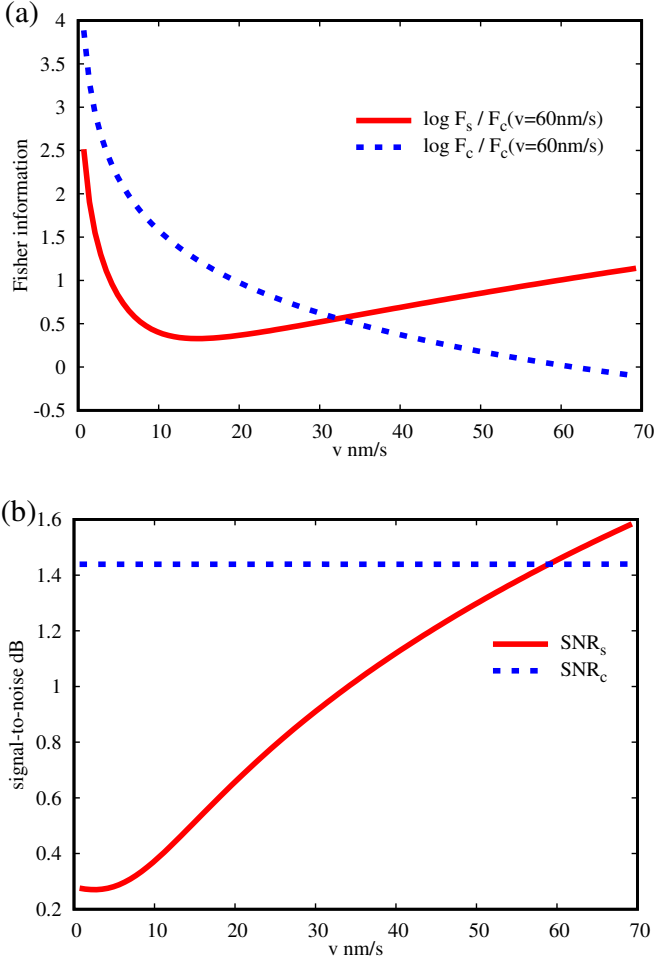


FIG. 6. The Fisher information (a) and the signal-to-noise (b) at different velocity with the traditional WVA technique and the modified WVA technique based on Vernier-effect.

$\mathbf{P}(x|\Omega)$ , the Fisher information[31] is defined as

$$\mathbf{F}(\Omega) = N \int dx \mathbf{P}(x|\Omega) \left[ \frac{d}{d\Omega} \ln \mathbf{P}(x|\Omega) \right]^2 \quad (14)$$

where  $N$  represents that  $N$  photons are sent through the interferometer. Then the  $CRB$ , which is the minimum variance  $\Delta^2(\Omega)$  of an unbiased of  $\Omega$  can be obtained as  $CRB=1/\mathbf{F}(\Omega)$ . Next, we calculate  $CRB$  and  $SNR$  in the TWVA technique and the MWVA technique based on Vernier-effect at the same measurement time  $0 < t < 4 \text{ ms}$  (discussed in Sec. III A). In our work, the parameter  $\Omega$  is corresponding to the temporal shift  $\delta t$ .

In the scheme of Fig. 1 with the traditional WVA technique, we chose the same pulse in Sec. III A and obtain the probability distribution of a random variable  $t$ :

$$\mathbf{P}_s = \begin{cases} \frac{(\sin\phi)^2}{\sqrt{0.32\pi}} e^{-(t-2.0+\delta t)^2/0.32} & t < 4\text{ms} \\ 0 & t > 4\text{ms} \end{cases}$$

and the Fisher information can be computed by

$$\mathbf{F}_s = N \int dt \mathbf{P}(t|\delta t) \left[ \frac{d}{d\delta t} \ln \mathbf{P}_s(t|\delta t) \right]^2 \quad (15)$$

The sensitivity in determination of  $\delta t = \frac{4\pi\tau^2 v}{\lambda\phi}$  is bounded by the square root of the minimum variance  $\Delta(\delta t) = \sqrt{1/\mathbf{F}_s}$ . And the smallest resolvable velocity is determined by the signal-to-noise

$$SNR_s = \frac{\delta t_s}{\Delta(\delta t)} = \frac{v}{\Delta v} = \frac{4v\pi\tau^2\sqrt{\mathbf{F}_s}}{\lambda\phi} \quad (16)$$

where  $\delta t_s = \delta t$ .

Meanwhile the Fisher information  $\mathbf{F}_c$  with the MWVA technique based on Vernier-effect in Fig. 3. To keep the same measurement times with the TWVA technique, we choose the input  $I_u^i$  (10) and  $I_d^i$  (12) with the same parameters in Sec. III A, then the Fisher information  $\mathbf{F}_c$  can be calculated by

$$\mathbf{F}_c = N \int dt \mathbf{P}(t|\delta t) \left[ \frac{d}{d\delta t} \ln \mathbf{P}_c(t|\delta t) \right]^2 \quad (17)$$

where the probability distribution  $\mathbf{P}_c$  satisfies:

$$\mathbf{P}_c = \begin{cases} \sum_{m=0}^N \frac{1}{\sqrt{0.08\pi}} [e^{-(t+46-2.00m+\delta t)^2/0.08} \\ + e^{-(t+46-1.96m+\delta t)^2/0.08}] & t < 4\text{ms} \\ 0 & t > 4\text{ms} \end{cases}$$

Therefore, the  $SNR_c$  is given by:

$$SNR_c = \frac{\delta t_c}{\Delta(\delta t)} = \frac{12v}{\Delta v} = \frac{48v\pi\tau^2\sqrt{\mathbf{F}_s}}{\lambda\phi} \quad (18)$$

where  $\delta t_c = 12\delta t$ . Note that the  $SNR_c$  with the TWVA technique will be enhanced with the factor  $eEnh = 12$  due to the Vernier-effect.

The complexity of the probability distribution  $\mathbf{P}_s$  and  $\mathbf{P}_c$  make it hard to analytically calculate the Fisher information. In our work, we numerically solve the integration (15) and the integration (17) for  $N = \times 10^6$ , and the results are shown in Fig. 6(a). And on this basis, we calculate the signal-to-noise at different velocities with the TWVA technique and the MWVA technique in Fig. 6(b).

In our work, the cramer-Rao bound( $CRB$ )[35, 36] states that the inverse of the Fisher information is a lower bound on the variance of any unbiased estimator of  $\delta t$ , by noting that  $\Delta^2(\delta t)$  characterizes the extent of the shot noise of the quantum measurement[19]. Firstly, the intuitive explanation for the Fisher Information is that the Fisher Information reflects the accuracy of our parameter estimation. The larger it is, the higher the accuracy of parameter estimation, that is, it represents more information. Fig. 6(a) shows that the Fisher Information  $\mathbf{F}_c$  with our MWVA technique is larger than  $\mathbf{F}_s$  with the traditional TWVA technique, when our measured velocity is less than 32 nm/s (read from Fig. 6(a)). However, with further increase of velocity  $v$ , our MWVA technique

will become less efficient than the TWVA technique. As we have pointed out, our MWVA technique is an effective alternative to the TWVA technique, when the measurement is beyond the limits of resolution of the detector in Fig. 1.

Let us continue the discussion related to the signal-to-noise in Fig. 6(b). The results show that the signal-to-noise  $SNR_c$  is larger than  $SNR_s$  with the traditional WVA technique. When our measured velocity is less than 58 nm/s (read from Fig. 6(b)). Note that an interesting conclusion can be drawn from Fig. 6. The Fisher information characterization is not fully equivalent to the SNR characterization with the increase of measurement velocity. And the similar conclusion is obtained by analyzing the WVA technique beyond the Aharonov-Albert-Vaidman limit in Ref [19]. In addition, as the measurement velocity is smaller, the signal-to-noise ratio of our MWVA technique is improved more.

We notice that the time shift  $\delta t_c$  in our MWVA technique is less than 3.5 ms thanks to ensuring the same time measurement window. And the upper limit of the corresponding velocity measurement is 40 nm/s. Therefore, we can conclude that our MWVA technique is more efficient than the TWVA technique, because  $SNR_c$  is larger than  $SNR_s$  as  $v < 40$  nm/s in Fig. 6(b).

#### IV. SUMMARY AND DISCUSSIONS

In summary, using the feature of sensitivity-enhanced in Vernier-effect, we have proposed a modified-weak-value-amplification(MWVA) technique of measuring the mirror's velocity. Compared with the traditional-weak-value-amplification(TWVA) technique, we demonstrated sensitivity-enhanced and higher SNR by using two cascaded Michelson interferometers. In our work, the two cascaded interferometers are composed of the similar optical structures. One interferometer with a fixed mirror acts as a fixed part of the Vernier-scale, while the other with a moving mirror acts as a sliding part of the Vernier-scale is for velocity sensing. By choosing the appropriate meter in our MWVA technique and in the TWVA technique to ensuring the same measurement time, we obtained numerical results of the sensitivity and the SNR in the two techniques.

Our numerical results show that our MWVA technique is more efficient than the traditional one with 12 times sensitivity-enhanced and higher SNR. In addition, as the measurement velocity is smaller, the SNR of our MWVA technique is improved more. Note that our MWVA technique can propose a viable and effective alternative for the measurement out of the limit of the resolution in the TWVA technique. In addition, by using the principles of the Vernier-effect, it is applicative and convenient to further improve the sensitivity and SNR in measuring other physical quantities with the WVA technique.

A few remarks are in order. We have proposed an intersecting-point-tracing(IPT) method for tracking the shift of the meter with cascaded Michelson interferometers, the IPT method indicates that the intersection of straight lines which is determined by interval troughs can track the shift of the envelope trough. It is remarked that we have found that the fisher information characterization is not fully equivalent to the SNR characterization with the increase of measurement velocity. And the conclusion is the response to the attention in Ref [19] from a purely theoretical interest.

In addition, our MWVA technique can be realized beyond the Gaussian meter wave function. Note that the work[37] shows that the Hermite-Gaussian and Laguerre-Gaussian pointer states for a given coupling direction have advantages and disadvantages over the fundamental Gaussian mode in improving the SNR. And the work[38] indicates that the post-selected weak measurement scheme for non-classical pointer states(coherent, squeezed vacuum, and Schrodinger cat states) to be superior to semi-classical ones. Therefore, a MWVA technique with a non-Gaussian meter wave function based on the Vernier-effect will be studied in our future works. Meanwhile, the relevant experiments are also being carried out gradually.

#### ACKNOWLEDGMENTS

This study is financially supported by the National Key Research and Development Program of China (Grant No. 2018YFC1503705) and the Fundamental Research Funds for National Universities, China University of Geosciences(Wuhan) (Grant No. G1323519204).

- 
- [1] F. Lecocq, L. Ranzani, G. A. Peterson, K. Cicak, X. Y. Jin, R. W. Simmonds, J. D. Teufel, and J. Aumentado, "Efficient qubit measurement with a nonreciprocal microwave amplifier," *Phys. Rev. Lett.* **126**, 020502 (2021).
  - [2] Jonathan T. Monroe, Nicole Yunger Halpern, Taeho Lee, and Kater W. Murch, "Weak measurement of a superconducting qubit reconciles incompatible operators," *Phys. Rev. Lett.* **126**, 100403 (2021).
  - [3] Yakir Aharonov, David Z. Albert, and Lev Vaidman, "How the result of a measurement of a component of the spin of a spin-1/2 particle can turn out to be 100," *Phys. Rev. Lett.* **60**, 1351-1354 (1988).
  - [4] Asher Peres, "Quantum measurements with postselection," *Phys. Rev. Lett.* **62**, 2326-2326 (1989).
  - [5] A. J. Leggett, "Comment on "how the result of a measurement of a component of the spin of a spin-(1/2) particle can turn out to be 100"," *Phys. Rev. Lett.* **62**, 2325-2325 (1989).
  - [6] J. S. Lundeen and A. M. Steinberg, "Experimental joint



- weak measurement on a photon pair as a probe of hardy's paradox," *Phys. Rev. Lett.* **102**, 020404 (2009).
- [7] Kazuhiro Yokota, Takashi Yamamoto, Masato Koashi, and Nobuyuki Imoto, "Direct observation of hardy's paradox by joint weak measurement with an entangled photon pair," *New Journal of Physics* **11**, 033011 (2009).
- [8] K.J. Resch, J.S. Lundeen, and A.M. Steinberg, "Experimental realization of the quantum box problem," *Physics Letters A* **324**, 125–131 (2004).
- [9] Daniel Rohrlich and Yakir Aharonov, "Cherenkov radiation of superluminal particles," *Phys. Rev. A* **66**, 042102 (2002).
- [10] Arnold Weissberger and Bryant W Rossiter, "Spectroscopy and spectrometry in the infrared, visible, and ultraviolet," *Nature* **474**, 188–91 (2011).
- [11] A. Szorkovszky, A. C. Doherty, G. I. Harris, and W. P. Bowen, "Mechanical squeezing via parametric amplification and weak measurement," *Phys. Rev. Lett.* **107**, 213603 (2011).
- [12] Omar S. Magaña Loaiza, Mohammad Mirhosseini, Brandon Rodenburg, and Robert W. Boyd, "Amplification of angular rotations using weak measurements," *Phys. Rev. Lett.* **112**, 200401 (2014).
- [13] Gang Li, Tao Wang, and He-Shan Song, "Amplification effects in optomechanics via weak measurements," *Phys. Rev. A* **90**, 013827 (2014).
- [14] L. Luo, Y. He, X. Liu, Z. Li, and Z. Zhang, "Anomalous amplification in almost-balanced weak measurement for measuring spin hall effect of light," *Optics Express* **28** (2020), 10.1364/OE.386017.
- [15] Huang.Jing-Hui, Duan. Xue-Ying, and Hu. Xiang-Yun, "Amplification of rotation velocity using weak measurements in sagnac's interferometer," *The European Physical Journal D* **75**, 114 (2021).
- [16] P. Ben Dixon, David J. Starling, Andrew N. Jordan, and John C. Howell, "Ultrasensitive beam deflection measurement via interferometric weak value amplification," *Phys. Rev. Lett.* **102**, 173601 (2009).
- [17] Gerardo I. Viza, Julián Martínez-Rincón, Gregory A. Howland, Hadas Frostig, Itay Shomroni, Barak Dayan, and John C. Howell, "Weak-values technique for velocity measurements," *Opt. Lett.* **38**, 2949–2952 (2013).
- [18] Arun Kumar Pati, Chiranjib Mukhopadhyay, Sagnik Chakraborty, and Sibasish Ghosh, "Quantum precision thermometry with weak measurements," *Phys. Rev. A* **102**, 012204 (2020).
- [19] Jianhua Ren, Lupei Qin, Wei Feng, and Xin-Qi Li, "Weak-value-amplification analysis beyond the aharonov-albert-vaidman limit," *Phys. Rev. A* **102**, 042601 (2020).
- [20] Shengshi Pang and Todd A. Brun, "Improving the precision of weak measurements by postselection measurement," *Phys. Rev. Lett.* **115**, 120401 (2015).
- [21] Tatsuhiko Koike and Saki Tanaka, "Limits on amplification by aharonov-albert-vaidman weak measurement," *Phys. Rev. A* **84**, 062106 (2011).
- [22] Shengshi Pang, Todd A. Brun, Shengjun Wu, and Zeng-Bing Chen, "Amplification limit of weak measurements: A variational approach," *Phys. Rev. A* **90**, 012108 (2014).
- [23] David J. Starling, P. Ben Dixon, Andrew N. Jordan, and John C. Howell, "Optimizing the signal-to-noise ratio of a beam-deflection measurement with interferometric weak values," *Phys. Rev. A* **80**, 041803 (2009).
- [24] Amir Feizpour, Xingxing Xing, and Aephraim M. Steinberg, "Amplifying single-photon nonlinearity using weak measurements," *Phys. Rev. Lett.* **107**, 133603 (2011).
- [25] Jingzheng Huang, Yanjia Li, Chen Fang, Hongjing Li, and Guihua Zeng, "Toward ultrahigh sensitivity in weak-value amplification," *Phys. Rev. A* **100**, 012109 (2019).
- [26] Courtney Krafczyk, Andrew N. Jordan, Michael E. Goggin, and Paul G. Kwiat, "Enhanced weak-value amplification via photon recycling," *Phys. Rev. Lett.* **126**, 220801 (2021).
- [27] Daoxin Dai, "Highly sensitive digital optical sensor based on cascaded high-q ring-resonators," *Opt. Express* **17**, 23817–23822 (2009).
- [28] Tom Claes, Wim Bogaerts, and Peter Bienstman, "Experimental characterization of a silicon photonic biosensor consisting of two cascaded ring resonators based on the vernier-effect and introduction of a curve fitting method for an improved detection limit," *Opt. Express* **18**, 22747–22761 (2010).
- [29] H. H. Zhu, Y. H. Yue, Y. J. Wang, M. Zhang, L. Y. Shao, J. J. He, and M. Y. Li, "High-sensitivity optical sensors based on cascaded reflective mzis and microring resonators," *Opt. Express* **25**, 28612–28618 (2017).
- [30] Yong Liu, Yang Li, Mingyu Li, and Jian-Jun He, "High-sensitivity and wide-range optical sensor based on three cascaded ring resonators," *Opt. Express* **25**, 972–978 (2017).
- [31] W. Hoyle, "Quantum measurement and control," *Electrical Engineers Journal of the Institution of* **2**, 28 (2010).
- [32] Nicolas Brunner and Christoph Simon, "Measuring small longitudinal phase shifts: Weak measurements or standard interferometry?" *Phys. Rev. Lett.* **105**, 010405 (2010).
- [33] Li-Yang Shao, Yuan Luo, Zhiyong Zhang, Xihua Zou, Bin Luo, Wei Pan, and Lianshan Yan, "Sensitivity-enhanced temperature sensor with cascaded fiber optic sagnac interferometers based on vernier-effect," *Optics Communications* **336**, 73–76 (2015).
- [34] Zeng, Shaoqun, Bi, Kun, Xue, Songchao, Liu, Yujing, Lv, and Xiaohua, "Acousto-optic modulator system for femtosecond laser pulses," *Rev. Sci. Instrum* **78**, 15103–15103 (2007).
- [35] B. Roy Frieden and Robert A. Gatenby, "Principle of maximum fisher information from hardy's axioms applied to statistical systems," *Phys. Rev. E* **88**, 042144 (2013).
- [36] Thorsten Pfister, Andreas Fischer, and Jürgen Czarske, "Cramér-rao lower bound of laser doppler measurements at moving rough surfaces," *Measurement Science and Technology* **22**, 055301 (2011).
- [37] Yusuf Turek, Hirokazu Kobayashi, Tomotada Akutsu, Chang-Pu Sun, and Yutaka Shikano, "Post-selected von neumann measurement with hermite-gaussian and laguerre-gaussian pointer states," *New Journal of Physics* **17**, 083029 (2015).
- [38] Yusuf Turek, W. Maimaiti, Yutaka Shikano, Chang-Pu Sun, and M. Al-Amri, "Advantages of nonclassical pointer states in postselected weak measurements," *Phys. Rev. A* **92**, 022109 (2015).